



Cite this: *Soft Matter*, 2023, 19, 6157

Many-body interactions between curvature-inducing membrane inclusions with arbitrary cross-sections

P. Galatola *^a and J.-B. Fournier ^b

By means of a multipolar expansion, we study analytically and numerically the interaction, in tensionless membranes, between multiple identical curvature-inducing membrane inclusions having arbitrary cross sections but uniform small detachment angles. In particular, for N circular inclusions forming regular polygons, we obtain analytical expressions for the total asymptotic interaction, up to $N = 6$, and we numerically compute the different multi-body contributions at arbitrary separations. We find that the latter are comparable to the sum of the two-body contributions. For $N = 5$ inclusions, the analytical asymptotic interaction scales as the inverse sixth power of the nearest neighbors distance d , weaker than the d^{-4} power for $N \neq 5$. The analytical interactions are always repulsive and in good agreement with the numerical results. In the case of noncircular cross sections, we consider the case of two identical inclusions having a given number of equally shaped lobes. Depending on the number of lobes and their amplitude, we find that the interaction is asymptotically either repulsive as d^{-4} or attractive as d^{-2} , and always repulsive at short distances. We also characterize how the interaction depends on the inclusion rotation angles in the membrane plane.

Received 28th June 2023,
Accepted 31st July 2023

DOI: 10.1039/d3sm00851g

rsc.li/soft-matter-journal

1. Introduction

Biological membranes consist of two layers of lipid molecules arranged in a tail-to-tail fashion, forming the structural barrier of our cells.¹ These membranes have a central hydrophobic core, and two outer hydrophilic layers, made by the lipid heads, which come into contact with the surrounding aqueous solvent. Some proteins are specifically designed to either fit inside the membrane or adhere to its surface. These include the so-called curvature-inducing proteins, which have the ability to bend the membrane so that it can accommodate their conical shape.²

The elastic energy of membranes is controlled by both lateral tension and bending rigidity, as described by Helfrich.³ Since curvature-inducing proteins deform membranes on a large scale, they experience long-range interactions mediated by the energy required for membrane deformation.⁴ The disk with detachment angle (DDA) model, introduced by Goulian *et al.*,^{4–6} was developed to investigate these effects. To describe the deformation caused by a protein, the section of the protein embedded in the hydrophobic membrane core is modeled as a disk of radius a , while the membrane, modeled as a surface, detaches from the disk at a

constant angle α . Multipolar expansion methods were used to obtain the leading-order asymptotic interaction between two inclusions.⁴ In a membrane with bending rigidity κ and negligible tension, two identical curvature-inducing inclusions separated by a distance d were found to repel each other with an asymptotic pairwise interaction energy given by $\mathcal{E} \simeq 8\pi\kappa\alpha^2(a/d)^4$. This interaction, obtained from a linearized calculation, is valid in the small detachment angle limit. Using effective field theory, Yolcu *et al.*^{7,8} calculated this interaction, for disks of different radii and detachment angles, up to order $(1/d)^6$. Using the original multipolar expansion method, we derived the interaction up to order $(1/d)^{14}$, making it possible to study how the series converges.⁹

Note that numerical studies, using triangulated surfaces energy minimization, have been used to explore the regime of large detachment angles, of inclusions with noncircular footprint, and of strongly curved membrane background.^{10–13} It was shown in particular that DDA-like inclusions with large detachment angle can attract each other when adsorbed on the outer side of strongly curved vesicles¹³ and that inclusions with crescent-like shapes experience strong attractions.¹²

Understanding the collective interactions of proteins in biological membranes at room temperature is crucial due to their abundance.¹ However, this poses three challenges: the weakness of the interactions at moderate distances, their multibody nature, and the noncircular shape of protein

^a Université Paris Cité, 10 rue Alice Domon et Léonie Duquet, F-75205 Paris Cedex 13, France. E-mail: paolo.galatola@u-paris.fr

^b Université Paris Cité, 10 rue Alice Domon et Léonie Duquet, F-75205 Paris Cedex 13, France



cross-sections (the non-uniformity of the detachment angle will not be addressed here). Let us discuss these points sequentially. Membrane typically have bending rigidities $\kappa \simeq 30k_B T$,¹ and curvature-inducing proteins can have detachment angles ranging from $\alpha \simeq 10^\circ$ to 35° . Indeed, while $a \simeq 5$ nm, spontaneous curvatures of $c \simeq (25\text{nm})^{-1}$ where measured for the KvaP channels² and $c \simeq (7\text{nm})^{-1}$ for BmrA in the ATP-blocked configuration.¹⁴ At a distance $d \simeq 6a$, where the spacing between the inclusions is large enough to hope that asymptotic expressions are reliable, the interaction energy is only $\mathcal{E} \simeq 0.1k_B T$. Therefore, relying on the first terms of the asymptotic expansion is not sufficient to investigate interactions that are significantly larger than $k_B T$. The range of applicability of the expansion to order $(1/d)^{14}$ is also uncertain. Therefore, in this paper, we conduct a numerical investigation of the interaction up to the point of contact. Specifically, we include up to 400 multipoles to obtain accurate results.

Using an approximate method based on the energy required to insert a protein into a curved background, Kim *et al.*¹⁵ have argued that multibody interactions are as significant as pairwise interactions. As shown by Yolcu *et al.*, this method correctly captures pairwise and triplet interactions, but neglects higher order multibody interactions.⁸ Therefore, little is known with certainty about membrane-mediated multibody interactions. In this paper, we use multipolar expansions to derive exact analytical expressions for the asymptotic many-body energy of clusters of up to six inclusions forming regular polygons. Our analysis highlights the relative amplitude of multibody terms. In particular, we show that pentagonal clusters have a small but nonzero many-body energy.¹⁵ Furthermore, we numerically calculate the many-body interaction energy of these clusters at very small separations between the inclusions.

Finally, the DDA model assumes the cross-section of the inclusion to be perfectly circular. Real proteins have an irregular shape, so it is important to know whether or not this changes the interaction, especially at short distances where this irregularity is significant. For example, as shown in ref. 8 and 9, the sixth order of the pairwise interaction between two identical perfectly circular disks vanishes. In this paper, we show that this is no longer the case if a shape modulation is present. We give general numerical results concerning the interaction between two curvature-inducing proteins with a noncircular cross-section in a tensionless membrane, discussing in particular the dependence of their interaction on their relative orientation.

Our paper is organized as follows. In Section 2 we review the multipolar method of Goulian *et al.*⁴ and we generalize it to inclusions of arbitrary contours. In Section 3 we apply this method to numerically compute the interaction between two identical circular inclusions and we compare the accurate numerical solution to the asymptotic analytical results. In Section 4 we obtain the leading asymptotic term of the interaction energy for $N = 3-6$ circular inclusions placed on a regular polygon. We compare this analytical results with numerical computations, and we extract from the latter the

various multi-body contributions. In Section 5, we study numerically the interaction between two identical noncircular inclusions having a variable number $\nu = 1-4$ of identical lobes. Finally, in Section 6, we summarize and discuss our results.

2. Interaction between arbitrarily shaped inclusions with a fixed detachment angle

We consider a bilayer lipidic membrane with no tension and zero spontaneous curvature, modeled as a geometric surface. We characterize the membrane shape in the Monge gauge by means of its height $z = h(x,y)$ above the reference plane (x,y) . For small deformations, the bending free energy of the membrane is given by³

$$\mathcal{F} = \frac{1}{2}\kappa \int (\nabla^2 h)^2 dx dy, \quad (1)$$

where κ is the bending energy, typically of the order of a few tens of the thermal energy $k_B T$, and the integral runs on the reference plane. Note that, in general, an extra contribution to the free energy, proportional to the integral of the Gaussian curvature, should be considered. However, this term only depends on the global topology of the membrane and on the integral of the geodesic curvature along the membrane contours. Therefore, for fixed membrane topologies and fixed membrane contours imposing local fixed detachment angles, the Gaussian free energy is a constant contribution that can be discarded. This is the case for our problem.

Minimizing the free energy F with respect to arbitrary deformations of the membrane height yields that the equilibrium membrane shape is solution of the biharmonic equation

$$\nabla^4 h = 0. \quad (2)$$

We suppose that N curvature-inducing inclusions, *e.g.* conical integral proteins or adhering colloids, are attached to the membrane. Generalizing the model of Goulian *et al.*⁴ to inclusions of non circular contours, we model each inclusion k as a planar contour of arbitrary shape from which the membrane detaches with a given fixed angle α_k (see Fig. 1). We associate to each inclusion k a reference point O_k of coordinates $x = x_k^0$, $y = y_k^0$, and $z = z_k^0$, lying in the plane of its contour, of normal $\hat{\nu}_k$. For each inclusion, we define a local coordinate system (x_k, y_k) in the reference plane, centered on the point (x_k^0, y_k^0) and possibly rotated with respect to the reference frame (x, y) , depending on the symmetry of the problem.

The orientation $\hat{\nu}_k$ of each inclusion is given by two angles β_k and γ_k . For small inclinations with respect to the reference plane, we set

$$\hat{\nu}_k = \hat{z} - \beta_k \hat{x}_k - \gamma_k \hat{y}_k, \quad (3)$$

where \hat{x}_k , \hat{y}_k , and \hat{z} are unit vectors in the direction of the corresponding axes. Note that, to first order in the angles β_k and γ_k , the projected shapes of the contours on the reference plane coincide with their actual shapes.



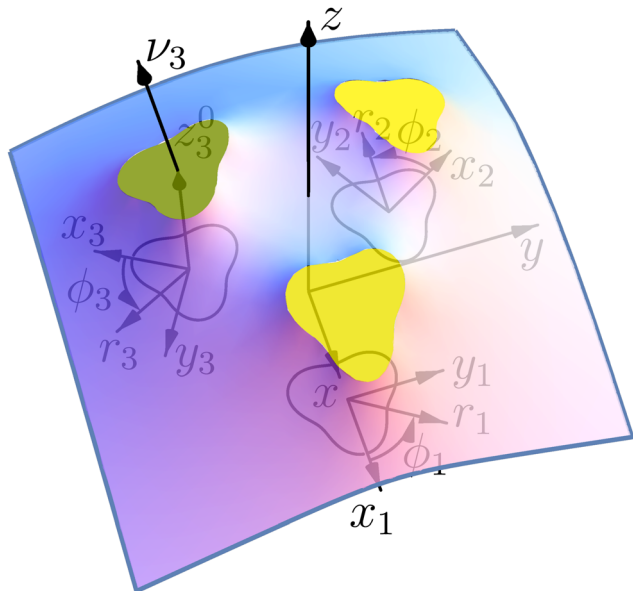


Fig. 1 Shape of a lipidic membrane around three identical curvature-inducing proteins with noncircular contours and uniform detachment angles. The coordinates used for describing the membrane geometry are shown (see Section 2).

With the first order approximation (3), the equation of the k contour's plane is $-\beta_k x_k - \gamma_k y_k + z - z_k^0 = 0$. Therefore, the condition that the inclusions are attached to the membrane gives, to first order in the inclinations, the boundary conditions

$$h(x_k, y_k) - \beta_k x_k - \gamma_k y_k|_{C_k} = z_k^0, \quad (4)$$

where $|_{C_k}$ indicates that the quantity on its left is evaluated along the projection of contour k on the reference plane. In the following, we will parametrize the latter contours as

$$r_k = r_k(\phi_k), \quad (5)$$

in terms of local polar coordinates (r_k, ϕ_k) on the reference plane, associated to the Cartesian coordinates (x_k, y_k) .

The detachment condition implies that the membrane height, measured from the plane of contour k , has derivative in the direction normal to the contour equal to $\tan \alpha_k$. Then, at first order in the inclinations β_k and γ_k and the detachment angles α_k , we have the boundary conditions

$$\frac{\partial}{\partial n_k} [h(x_k, y_k) - \beta_k x_k - \gamma_k y_k] = \alpha_k, \quad (6)$$

where $\partial/\partial n_k$ indicates the derivative in the direction \hat{n}_k of the outward normal to the contour $r_k = r_k(\phi_k)$:

$$\frac{\partial}{\partial n_k} = \frac{r_k \frac{\partial}{\partial r_k} \Big|_{C_k} - \frac{1}{r_k} \frac{dr_k}{d\phi_k} \frac{\partial}{\partial \phi_k} \Big|_{C_k}}{\sqrt{r_k^2 + \left(\frac{dr_k}{d\phi_k}\right)^2}}. \quad (7)$$

Note that the equilibrium free energy (1) can be expressed, by using two integrations by parts and the equilibrium condition (2), as the sum of line integrals along the contours C_k of the

inclusions:

$$\mathcal{F} = \frac{1}{2} \kappa \sum_{k=1}^N \oint_{C_k} \left[h \frac{\partial}{\partial n_k} (\nabla^2 h) - (\nabla^2 h) \frac{\partial h}{\partial n_k} \right] ds_k, \quad (8)$$

where ds_k is the elementary arc length

$$ds_k = \sqrt{r_k^2 + \left(\frac{dr_k}{d\phi}\right)^2} d\phi_k. \quad (9)$$

Finally, the interaction energy \mathcal{E} between the inclusions is the difference between the free energy \mathcal{F} and the sum of the free energies of each isolated inclusion.

2.1 Multipolar expansion

Even for two inclusions with circular contours, the boundary problem (2), (4), (6) cannot be exactly solved analytically. Goulian *et al.*, by means of a multipolar expansion, first obtained⁴⁻⁶ an asymptotic expression for the interaction free energy of two identical circular inclusions of radii a , valid to fourth order in the ratio between a and their distance d .

The next to leading, sixth order, asymptotic term for two different circular inclusions was derived by Yolcu *et al.* using effective field theory.^{7,8} Higher-order terms, up to fourteen order, were successively obtained by us,⁹ using the original multipolar technique.

To solve our boundary problem for N inclusions, similarly to ref. 4, 9 and 16, we look for a solution of the biharmonic equation (2) in the form of the multipolar expansion:

$$h = L \sum_{k=1}^N \left\{ A_{k,0}^c \log \bar{r}_k + \frac{A_{k,1}^c}{\bar{r}_k} \cos \phi_k + \frac{A_{k,1}^s}{\bar{r}_k} \sin \phi_k + \sum_{m=2}^{\infty} \left[\left(\frac{A_{k,m}^c}{\bar{r}_k^m} + \frac{B_{k,m}^c}{\bar{r}_k^{m-2}} \right) \cos(m\phi_k) + \left(\frac{A_{k,m}^s}{\bar{r}_k^m} + \frac{B_{k,m}^s}{\bar{r}_k^{m-2}} \right) \sin(m\phi_k) \right] \right\}, \quad (10)$$

where L is some characteristic length of the problem, that we use for dimensionalization purposes, and $\bar{r}_k = r_k/L$. The constant coefficients $A_{k,m}^c$ and $A_{k,m}^s$ (resp. $B_{k,m}^c$ and $B_{k,m}^s$) multiply elementary solutions of the biharmonic eqn (2) having vanishing (resp. non vanishing) Laplacian. Up to a constant term, eqn (10) is the sum of all the elementary separated solutions in polar coordinates of the biharmonic eqn (2) that are singular only at the centers $r_k = 0$ of the inclusions and that tend to a flat shape parallel to the reference plane at infinity. Note that not including in eqn (10) the elementary solutions of the biharmonic equation that have divergent curvatures at infinity implies that, on each inclusion, the force normal to the reference plane and the torques parallel to the latter identically vanish (see Appendix A).

The unknown expansion coefficients in eqn (10) are uniquely determined by the boundary eqn (4) and (6). Indeed, truncating the expansion (10) to a maximum order $m = M$, yields, for $M \geq 2$, $N(4M - 1)$ unknowns. Expanding eqn (4) and (6), for each inclusion k , as Fourier series relative to the angle ϕ_k , truncated to the same maximum harmonic M , gives $4M + 2$



equations for each inclusion. However, the boundary conditions contain, for each inclusion, the three extra unknowns β_k , γ_k (the inclusion tilts) and z_k (the inclusion height). Thus, we have a total number of unknowns $N(4M + 2)$ that equals the number of boundary conditions. In practice, it is simpler to disregard the zeroth harmonics of eqn (4) from the boundary equations, along with the corresponding unknowns heights z_k . Then, we are left with only $N(4M + 1)$ equations and the same number of unknowns. The remaining unknown heights z_k can be determined, once the full solution h is computed, by evaluating the zeroth harmonics of the left-hand side of eqn (4).

3. Numerical solution for two circular inclusions

We start by considering two identical circular inclusions of radius a separated by a center-to-center distance d . We put the projection on the reference plane of the center of inclusion 1 (resp. 2) at $x = -d/2, y = 0$ (resp. $x = d/2, y = 0$) and we define the local Cartesian coordinates

$$x_1 = x + \frac{d}{2}, \quad y_1 = y, \quad (11)$$

$$x_2 = -x + \frac{d}{2}, \quad y_2 = -y, \quad (12)$$

such that the frame (x_2, y_2) is obtained from (x_1, y_1) by means of a rotation of angle π around the midpoint of the segment joining the centers of the two inclusions. Then, the polar coordinates associated to the two Cartesian frames are related by the transformations

$$r_2 = \sqrt{r_1^2 + d^2 + 2dr_1 \cos \phi_1}, \quad (13)$$

$$\phi_2 = \arctan(r_1 \cos \phi_1 - d, r_1 \sin \phi_1) - \pi, \quad (14)$$

where $\arctan(x, y)$ is the polar angle of the point (x, y) . The inverse transformations are obtained by the exchanges $r_1 \leftrightarrow r_2$, $\phi_1 \leftrightarrow \phi_2$.

By symmetry, $A_{1,m}^c = A_{2,m}^c$, $B_{1,m}^c = B_{2,m}^c$, and $\beta_1 = \beta_2$, while, for $k = 1, 2$, all the $A_{k,m}^s$ and $B_{k,m}^s$ coefficients vanish, as well as the tilt angles γ_k . We determine numerically all the remaining independent coefficients up to the maximum order $m = M$ by means of a Fast Fourier Transform (FFT) of the boundary conditions (4) and (6) on one of the two inclusions. To avoid aliasing effects, the FFT is computed up to a sufficiently high harmonic $P \gg M$ and we impose the boundary conditions only on the $1, 2, \dots, M$ cosine harmonics of eqn (4) and the $0, 1, 2, \dots, M$ cosine harmonics of eqn (6) on one of the two boundaries. We then solve numerically the resulting system of $2M + 1$ linear equations for the $2M + 1$ independent unknowns $A_{1,0}^c, A_{1,1}^c, A_{1,2}^c, B_{1,2}^c, \dots, A_{1,M}^c, B_{1,M}^c, \beta_1$. Once the latter are determined, we compute the membrane free energy (8) by taking the zeroth harmonic of the integrand with respect to ϕ_1 of eqn (8) and (9). By increasing the maximum order M

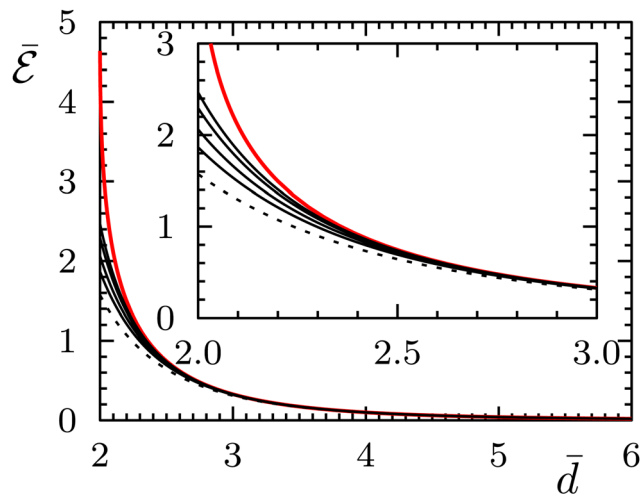


Fig. 2 Normalized interaction energy $\bar{\mathcal{E}} = \mathcal{E}/(\kappa a^2)$ as a function of the normalized center-to-center distance $\bar{d} = d/a$ for two identical circular inclusions. The upper thicker red curve is the exact interaction computed numerically up to the maximum multipolar order $M = 200$. The thinner black curves are the analytical asymptotic expansions up to order n , with $n = 4$ (dotted line), 8, 10, 12, 14 from bottom to top. The inset shows a magnification close to the contact $\bar{d} = 2$.

(together with P), we check for the convergence of the free energy interaction.

In Fig. 2 we show the normalized interaction energy $\bar{\mathcal{E}} = \mathcal{E}/(\kappa a^2)$ as a function of the normalized distance $\bar{d} = d/a$ between the centers of the inclusions (upper red curve). Note that the free energy of an isolated circular inclusion is zero: therefore the interaction energy \mathcal{E} coincides with \mathcal{F} . To obtain a relative error of the order of 10^{-3} at contact ($\bar{d} = 2$) we set $M = 200$ and $P = 2^{10}$. Note that, for $\bar{d} > 2$, the relative error rapidly decreases. On the same curve, we show also the analytical asymptotic expansions at order $n = 4, 8, 10, 12, 14$ obtained in ref. 9. For $\bar{d} > 2.5$, the $n = 14$ approximation is excellent, while at smaller separation higher-order corrections are needed. For $\bar{d} > 3$, the lowest order approximation $n = 4$ is sufficient. However, as we will see, when multiple or noncircular inclusions are present, the asymptotic interaction does not, in general, faithfully represent the actual interaction at such short separations.

4. N circular inclusions on a regular polygon

To study the importance of multibody interactions, we consider $N > 2$ identical inclusions with circular cross sections of radius a and centers arranged on a regular polygon:

$$x_k^0 = R \cos\left(\frac{2\pi k}{N}\right), \quad (15)$$

$$y_k^0 = R \sin\left(\frac{2\pi k}{N}\right), \quad (16)$$

where R is the radius of the circle circumscribed to the regular



polygon and $k = 0, 1, \dots, N - 1$. As for two identical inclusions, we rotate the local coordinate system centered on inclusion k by the angle $2\pi k/N$, in such a way that the x_k direction coincides with the direction joining the center of the polygon to the center of inclusion k , as shown in Fig. 1 for noncircular inclusions. Then, by symmetry, for any k and ℓ , $A_{k,m}^c = A_{\ell,m}^c$, $B_{k,m}^c = B_{\ell,m}^c$, $\beta_k = \beta_\ell$, while all the $A_{k,m}^s$ and $B_{k,m}^s$ coefficients vanish, as well as the tilt angles γ_k .

Following ref. 9, for each inclusion k , we introduce the normalized complex coordinate on the reference plane

$$z_k = \bar{r}_k \exp(i\phi_k), \quad (17)$$

where i is the imaginary unit and we normalize the lengths with respect to R . Then, the transformations of coordinates between the local coordinates centered on the inclusions are, in complex notation,

$$z_k = (z_0 + 1) \exp\left(-\frac{2\pi ik}{N}\right) - 1. \quad (18)$$

With the given symmetry and the complex coordinates, the multipolar expansion (10) can be written as the real part of the complex function

$$\eta = R \sum_{k=0}^{N-1} \left[A_0 \log z_k + \frac{A_1}{z_k} + \sum_{m=2}^{\infty} \left(\frac{A_m}{z_k^m} + \frac{B_m z_k^*}{z_k^{m-1}} \right) \right], \quad (19)$$

where z_k^* denotes the complex conjugate of z_k .

By symmetry, it is enough to impose the boundary conditions (4) and (6) on the reference inclusion 0. This can be done analytically by injecting the transformations (18) in the complex function (19), truncating the multipoles to a maximum order $m = M$, and expanding in Taylor series around $z_0 = 0$ the terms of the function η with $k = 1, 2, \dots, N - 1$, regarded as analytical functions of z_0 for fixed z_k^* . Taking the real part of η and going back to the polar coordinates \bar{r}_0 and ϕ_0 , we obtain an expansion of h in the form of a Fourier series in $\cos(m\phi_0)$, where each Fourier coefficient depends on the coordinate \bar{r}_0 and the amplitudes $A_{m'}$ and $B_{m'}$, with $m' = 0, 1, \dots, M$. The boundary conditions (4) and (6) on the reference inclusion 0 ($\bar{r}_0 = a/R$) give then a linear system of $2M$ equations in the $2M$ unknowns $A_0, A_1, A_2, B_2, \dots, A_M, B_M$, that we solve to the lowest order in a/R giving a nonzero interaction energy. For $N = 2, 3, 4, 5, 6$ we find $A_0 = \alpha a/R$, while the next nonzero multipolar coefficients at lowest order, B_2 and B_3 , are given in Table 1, along with the corresponding interaction energies. The latter, since the inclusions are circular, coincide with the free energy (8)–(9). Note that, generalizing our numerical solution to the case of N identical circular inclusions, we recover numerically the same asymptotic behavior. As one can see, except for $N = 5$, the next leading nonzero coefficient after A_0 is $B_2 \propto (a/R)^3$, giving an interaction free energy $\propto (a/R)^4$. For $N = 5$, the next leading coefficient is $B_3 \propto (a/R)^5$ and the corresponding interaction free energy is only $\propto (a/R)^6$. Note that, contrary to Kim *et al.*,¹⁵ we find that the interaction energy of five identical circular inclusion in a regular pentagonal arrangement is nonzero. Actually, this result is not in contradiction with

Table 1 Multipolar coefficients B_2 and B_3 and interaction energy \mathcal{E} at lowest order in a/R as a function of the number N of equal inclusions on a regular polygon. Note that the distance d between the centers of the nearest-neighbor inclusions is $R\sqrt{2(1 - \cos(2\pi/N))}$

N	B_2	B_3	\mathcal{E}
2	$\alpha \left(\frac{a}{R}\right)^3$	0	$\frac{1}{2} \pi \kappa \alpha^2 \left(\frac{a}{R}\right)^4$
3	$\frac{1}{3} \alpha \left(\frac{a}{R}\right)^3$	0	$\frac{4}{3} \pi \kappa \alpha^2 \left(\frac{a}{R}\right)^4$
4	$\frac{1}{4} \alpha \left(\frac{a}{R}\right)^3$	0	$\pi \kappa \alpha^2 \left(\frac{a}{R}\right)^4$
5	0	$\alpha \left(\frac{a}{R}\right)^5$	$40 \pi \kappa \alpha^2 \left(\frac{a}{R}\right)^6$
6	$-\frac{5}{12} \alpha \left(\frac{a}{R}\right)^3$	0	$\frac{25}{6} \pi \kappa \alpha^2 \left(\frac{a}{R}\right)^4$

ref. 15, since, as pointed out by ref. 8, the result of ref. 15 takes into account only pairwise and triplet interactions up to terms scaling with the distance as $(a/R)^4$. Our result, on the other hand, takes into account all the multibody interactions and captures in a controlled way the leading contribution to the interaction in powers of a/R . In agreement with ref. 15 and 8, we can then conclude that, asymptotically, multibody interactions are as significant as the pairwise ones: indeed, for $N = 5$ the sum of the pairwise interactions scales as $(a/R)^4$, and, for instance, for $N = 3$, as can be easily checked, the sum of the pairwise interactions is the double of the total many-body interaction.

4.1 Multibody interactions

To assess the relevance of multibody interactions at any separation, we determine numerically the full many-body interaction \mathcal{E} of N identical circular inclusions on a regular polygon, along with the p -body contributions \mathcal{E}_p , with $p = 2, 3, \dots, N$. For p inclusions $1, 2, \dots, p$ chosen between the N , \mathcal{E}_p is defined recursively as

$$\mathcal{E}_p(1, 2, \dots, p) = \mathcal{E}(1, 2, \dots, p) - \sum_{k=2}^{p-1} \sum_{\{c_1, c_2, \dots, c_k\}} \mathcal{E}_k(c_1, c_2, \dots, c_k), \quad (20)$$

where $\mathcal{E}(1, 2, \dots, p)$ is the full many-body interaction between the p inclusions $1, 2, \dots, p$ and the innermost sum at the right-hand side of eqn (20) runs over all the different way of choosing $2 \leq k < p$ inclusions c_1, c_2, \dots, c_k between the p inclusions. For instance, for three inclusions, the three-body interaction between the three inclusions is the full many-body interaction of the three inclusions minus the sum of the three two-body interactions between the three different pairs of inclusions. Similarly, for four inclusions, the four-body interaction between the four inclusions is the full many-body interaction of the four inclusions, minus the sum of the four three-body interactions between the four different triplets of inclusions, minus the sum of the six two-body interactions between the six different pairs of inclusions.

Finally, we define the total p -body contribution $\mathcal{E}^{(p)}$ to the interaction energy as the sum of all the p -body contributions



over all the possible ways of choosing p inclusions between the N :

$$\mathcal{E}^{(p)} = \sum_{\{c_1, c_2, \dots, c_p\}} \mathcal{E}_p(c_1, c_2, \dots, c_p). \quad (21)$$

Then, according to eqn (20), the full many-body interaction is equal to the sum of the total p -body contributions:

$$\mathcal{E} = \sum_{p=2}^N \mathcal{E}^{(p)}. \quad (22)$$

Fig. (3)–(6) show, for $N = 3$ – 6 identical inclusions on a regular polygon, the full many-body normalized interaction $\bar{\mathcal{E}} = \mathcal{E}/(\kappa\alpha^2)$ together with the various total multi-body contributions $\bar{\mathcal{E}}^{(p)}$ for the interaction index $p = 2, \dots, N$. The three and higher multi-body contributions are attractive and considerably reduce the two-body repulsion (except, possibly, for some contributions very close to contact). This confirms the result of Kim *et al.*¹⁵ that nonpairwise multi-body interactions are comparable to the pairwise ones, even though their magnitude decreases with their index p , except very close to contact. The black dotted curves in Fig. (3)–(6) are the analytical asymptotic full many-body interactions given in Table 1. As it is apparent, for $N = 3$ and $N = 5$ these approximations are actually quite good even rather close to the contact, while for $N = 4$ and $N = 6$ (and, to a certain degree, for $N = 2$, see Fig. 2) the approximation holds only asymptotically ($\bar{d} > 10$). Thus, the leading asymptotic term captures the relevant nonpairwise interactions and is more accurate than the total two-body (pairwise) interaction,

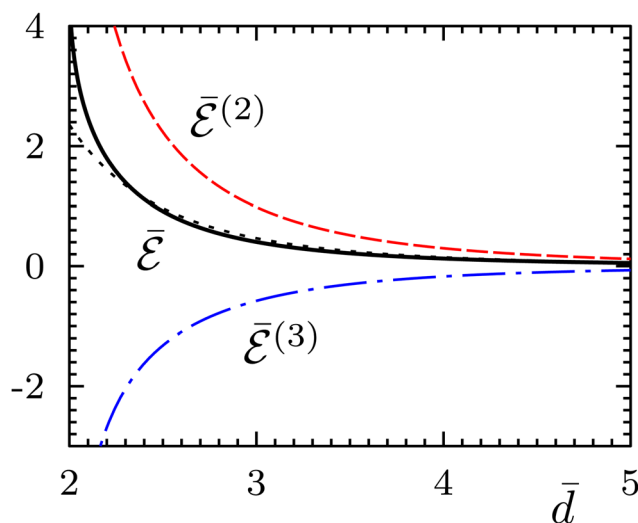


Fig. 3 Normalized total many-body interaction $\bar{\mathcal{E}}$ (black solid line), along with the total normalized two-body interaction energy $\bar{\mathcal{E}}^{(2)}$ (red dashed line) and the total normalized three-body interaction $\bar{\mathcal{E}}^{(3)}$ (blue long dashed-dotted line) for three inclusions on a regular polygon as a function of the normalized distance $\bar{d} = d/a$ between the centers of two neighbor inclusions. The black dotted curve is the analytical asymptotic expression $\bar{\mathcal{E}} = 12\pi/\bar{d}^4$ (see Table 1). The interaction energies are normalized with respect to $\kappa\alpha^2$. Note that, by definition, $\bar{\mathcal{E}} = \bar{\mathcal{E}}^{(2)} + \bar{\mathcal{E}}^{(3)}$.

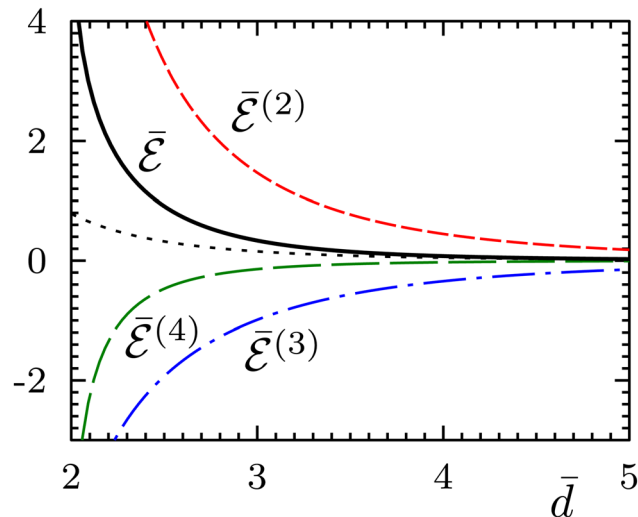


Fig. 4 Same as Fig. 3 but for four inclusions on a regular polygon. The total normalized four-body interaction is $\bar{\mathcal{E}}^{(4)}$ (green long-dashed line). The analytical asymptotic expression (black dotted curve) is $\bar{\mathcal{E}} = 4\pi/\bar{d}^4$ (see Table 1). Note that, as in Fig. 3 and in the following two figures, $\bar{\mathcal{E}} = \sum_p \bar{\mathcal{E}}^{(p)}$.

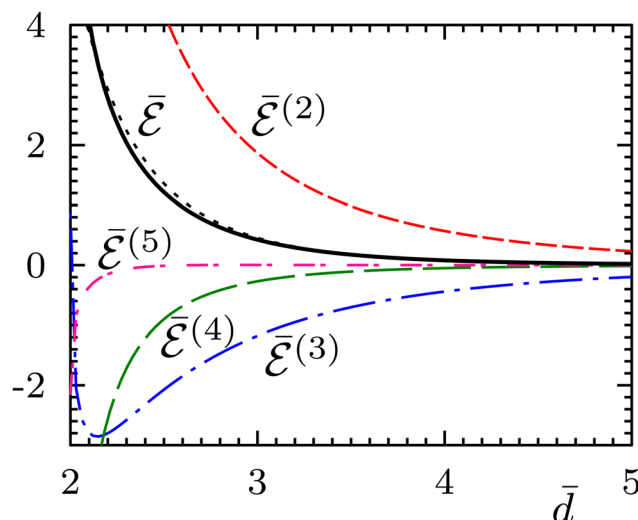


Fig. 5 Same as Fig. 4 but for five inclusions on a regular polygon. The total normalized five-body interaction is $\bar{\mathcal{E}}^{(5)}$ (pink short dashed-dotted line). The analytical asymptotic expression (black dotted curve) is $\bar{\mathcal{E}} = 5(5 - \sqrt{5})^3 \pi/\bar{d}^6$ (see Table 1).

even though it is not always quite reliable at distances comparable to the sizes of the inclusions.

5. Interaction between two identical noncircular inclusions

Since real proteins have irregular shapes, it is important to know how the interaction energy is affected by modifications to



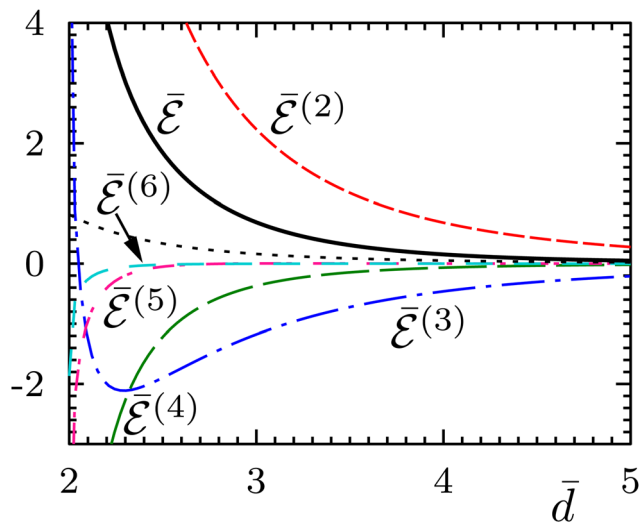


Fig. 6 Same as Fig. 5 but for six inclusions on a regular polygon. The total normalized six-body interaction is $\bar{\mathcal{E}}^{(6)}$ (turquoise dashed-spaced line). The analytical asymptotic expression (black dotted curve) is $\bar{\mathcal{E}} = 25\pi/(6\bar{d}^4)$ (see Table 1).

the circular contour case. As discussed in Section 2, for the sake of simplicity, we assume that the detachment angle is constant along the contour of the inclusions. We consider two identical inclusions, the contours of which we model by the parametric shapes:

$$\bar{r}_k(\phi_k) = 1 + \varepsilon \cos[\nu(\phi_k - \psi_k)], \quad (23)$$

where $k = 1$ ($k = 2$) for the left (right) inclusion. Here, \bar{r}_k and ϕ_k are polar coordinates centered on inclusion k , with the radial coordinates \bar{r}_k normalized with respect to the average radius a of the inclusions and the angles ϕ_k counted counterclockwise starting from the segment joining the centers of the two inclusions (see Fig. 7), $0 < \varepsilon < 1$ is the amplitude of the modulation from a circular shape, $\nu = 1, 2, \dots$ is an integer that counts the number of lobes of the shape, and $-\pi/\nu \leq \psi_k \leq \pi/\nu$ gives the orientation of inclusion k . Note that for $\nu = 1$, although at lowest order in $\varepsilon \ll 1$ the shape (23) corresponds to a simple

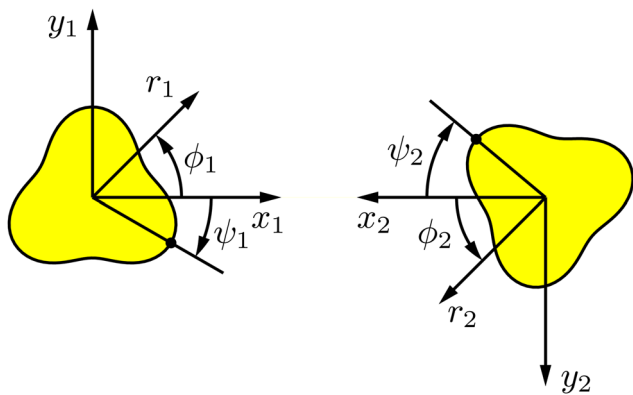


Fig. 7 Local coordinates used to describe the geometry of two noncircular inclusions. The angular coordinate ϕ_1 (resp. ϕ_2) is counted counterclockwise from the x_1 (resp. x_2) axis.

translation of a circular contour, for a finite moderate ε the contour is flattened around $\phi_k = \psi_k + \pi$.

To study the interaction between the two inclusions, we analyze, for a fixed distance \bar{d} between the centers of the two inclusions, the behavior of the interaction energy $\bar{\mathcal{E}} = \mathcal{E}/(\kappa\alpha^2)$ as a function of the two orientation angles ψ_1 and ψ_2 . Note that, rotating by π the system in the reference plane about the midpoint between the two inclusions corresponds to the interchange $\psi_1 \leftrightarrow \psi_2$, implying the symmetry $\bar{\mathcal{E}}(\psi_1, \psi_2) = \bar{\mathcal{E}}(\psi_2, \psi_1)$. Furthermore, turning the membrane upside-down with respect to the direction normal to the reference plane corresponds to the transformation $\psi_k \leftrightarrow -\psi_k$, $\alpha \leftrightarrow -\alpha$. Since the energy is invariant with respect to the sign of α , this implies the symmetry $\bar{\mathcal{E}}(\psi_1, \psi_2) = \bar{\mathcal{E}}(-\psi_2, -\psi_1)$. Taking into account these symmetries and the polar angle periodicity $2\pi/\nu$ of the shapes (23), we represent all the non equivalent angular configurations of the two inclusions by the combinations $\sigma = \frac{1}{2}(\psi_1 + \psi_2)$ and $\delta = \frac{1}{2}(\psi_1 - \psi_2)$, with $0 \leq \sigma, \delta \leq \pi/\nu$ and $\sigma + \delta \leq \pi/\nu$. Note that the points $(\sigma = \pi/\nu, \delta = 0)$ and $(\sigma = 0, \delta = \pi/\nu)$ are the only two points that actually correspond to the same configuration.

5.1 One lobe

We start by considering the slightly flattened shapes (23) for $\nu = 1$ and $\varepsilon = 0.4$. Fig. 8 shows the contour plot of the interaction energy $\bar{\mathcal{E}}$ as a function of the angles σ and δ for the normalized

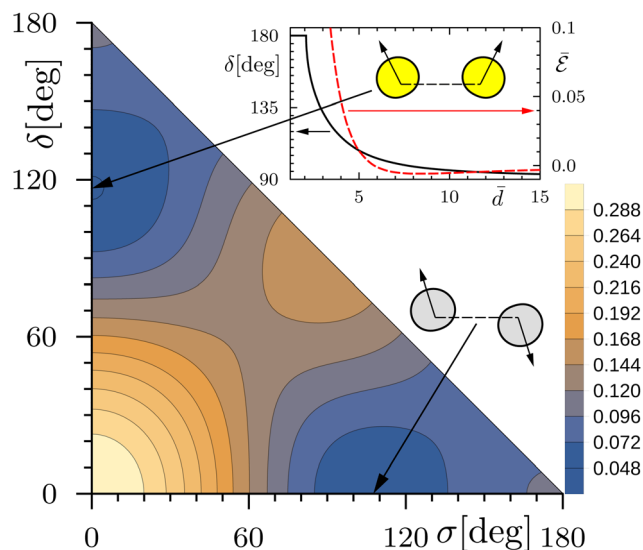


Fig. 8 Contour plot of the normalized interaction energy $\bar{\mathcal{E}}$ of two noncircular inclusions, for $\nu = 1$, $\varepsilon = 0.4$ and $\bar{d} = 4$, as a function of the rotation angles $\sigma = \frac{1}{2}(\psi_1 + \psi_2)$ and $\delta = \frac{1}{2}(\psi_1 - \psi_2)$. The inset shows the rotation angle δ minimizing the interaction energy as a function of the normalized distance \bar{d} (black solid line and left vertical scale), along with the corresponding normalized interaction energy $\bar{\mathcal{E}}$ (red dashed line and right vertical scale). The shapes and orientations of the two inclusions at the absolute (resp. relative) minimum for $\bar{d} = 4$ are shown in yellow (resp. gray). The orientations ψ_i ($i = 1, 2$) of the inclusions are indicated by arrows centered on the inclusions.



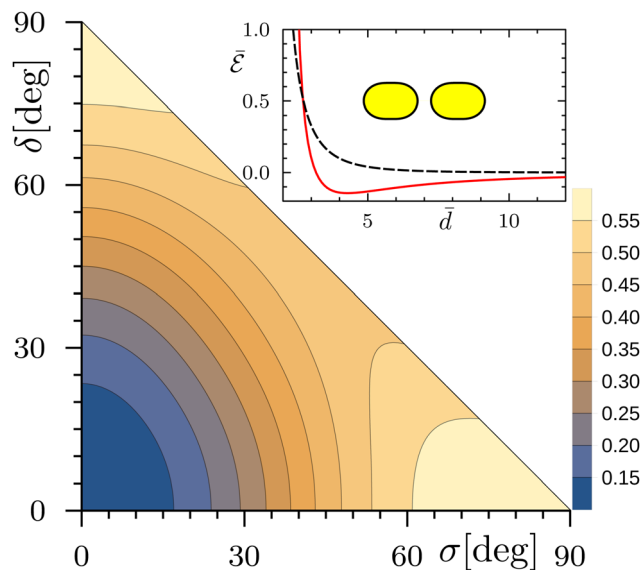


Fig. 9 Contour plot of the normalized interaction energy $\bar{\mathcal{E}}$ of two noncircular inclusions, for $\nu = 2$, $\varepsilon = 0.2$ and $\bar{d} = 3$, as a function of the rotation angles $\sigma = \frac{1}{2}(\psi_1 + \psi_2)$ and $\delta = \frac{1}{2}(\psi_1 - \psi_2)$. The red continuous line in the inset shows the normalized interaction energy $\bar{\mathcal{E}}$ as a function of the normalized distance \bar{d} for the orientation $\psi_1 = \psi_2 = 0$ corresponding to the minimum interaction energy. The latter orientation is shown inside the inset. The black dashed line in the inset is the normalized interaction energy for two circular inclusions with the same average radius ($\varepsilon = 0$).

distance $\bar{d} = 4$. Here and in the following Fig. 9–12, we set the maximum multipolar order M to 40, such that the numerical errors are negligible with respect to the used scales. The energy landscape presents two relative minima on the axes $\sigma = 0$ and $\delta = 0$, with the first one corresponding to the absolute minimum. The configurations of the two inclusions at the two minima are shown in the figure. As the inclusions move farther apart, the two minima remain on the axes $\sigma = 0$ and $\delta = 0$, continuously

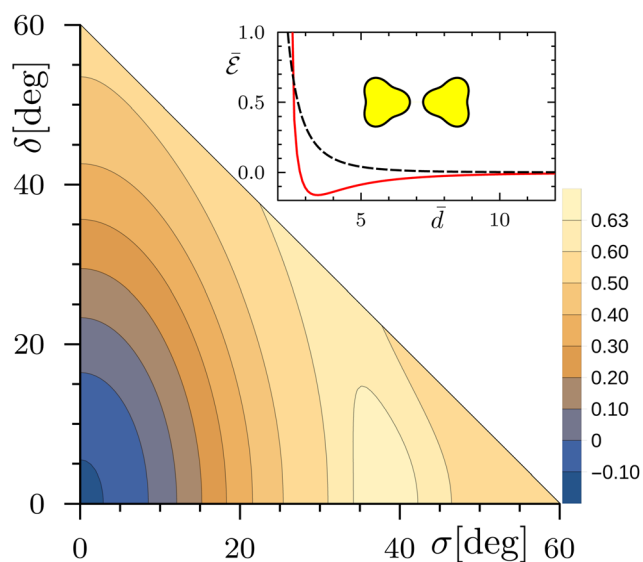


Fig. 10 Same as Fig. 9 but for $\nu = 3$.

shifting towards the positions $\delta = \pi/2$ and $\sigma = \pi/2$, respectively. For closer distances, the positions of the minima remain on the same axes and tend to $\delta = \pi$ and $\sigma = \pi$, reaching the limiting values at a finite short distance $\bar{d} \approx 2.1$. These two corner points of the contour plot, as we pointed out before, actually correspond to the same configuration, having the flattened sides of the inclusions facing each other. Note that, in this configuration, the normalized contact distance is $\bar{d} = 2(1 - \varepsilon)$, corresponding to $\bar{d} = 1.2$ in Fig. 8.

The inset of Fig. 8 shows the angle δ of the absolute minimum as a function of the distance \bar{d} and the corresponding interaction energy $\bar{\mathcal{E}}$. At large distances, the interaction is weakly attractive and decays as $1/d^2$, as we checked numerically. This asymptotic attractive behavior holds for any value of ε . As $\varepsilon \rightarrow 0$, the position of the energy minimum shifts toward $\bar{d} \rightarrow \infty$ and, correspondingly, its depth tends to zero. At short separations, the interaction becomes repulsive.

5.2 Two lobes

For $\nu = 2$ and moderate values of ε , the shapes (23) are elongated as a capsule in the two opposite directions $\phi_k = \psi_k$ and $\phi_k = \psi_k + \pi$ (see inset of Fig. 9). Taking $\varepsilon = 0.2$, we find that at all distances there is only a single minimum at $\sigma = \delta = 0$ (see Fig. 9), corresponding to the configuration in which the tips of the two inclusions face each other. Again, at large distances the interaction is asymptotically attractive as d^{-2} , behaving similarly for $\varepsilon \rightarrow 0$, and it becomes repulsive at short separations.

5.3 Three lobes

For $\nu = 3$ and the same value $\varepsilon = 0.2$, we find again that the configuration minimizing the free energy corresponds to the tips of the inclusions facing each other (see Fig. 10). The interaction energy as a function of the distance \bar{d} and of the modulation amplitude ε has the same qualitative behavior as for $\nu = 2$.

5.4 Four lobes

A qualitatively different behavior appears for $\nu = 4$ and small ε deformations. Indeed, as shown in Fig. (11) for $\varepsilon = 0.1$, while the configuration minimizing the free energy still corresponds to the tips of the inclusions facing each other, the interaction is now always repulsive. We check that the interaction $\bar{\mathcal{E}}$ decays at large distances as d^{-4} , as for circular contours, by verifying numerically that $\bar{\mathcal{E}}\bar{d}^4$ tends to a constant value c_4 for large \bar{d} . Then, to find the next to leading asymptotic contribution to the free energy, we plot in log–log scale the difference $c_4 - \bar{\mathcal{E}}\bar{d}^4$ as a function of the distance \bar{d} . As shown in Fig. 12, the latter difference scales as \bar{d}^{-2} , showing that $\bar{\mathcal{E}} = c_4/\bar{d}^4 + c_6/\bar{d}^6 + \dots$. Thus, at variance with perfect circular inclusions,^{7,9} a non-zero \bar{d}^{-6} asymptotic contribution is now present. Increasing ε , at $\varepsilon \approx 0.15$ an inflection point in the $\bar{\mathcal{E}}(\bar{d})$ graph appears at $\bar{d} \approx 5$, that splits, as ε further increases, into a pair of relative extrema: a minimum followed at a larger distance by a maximum. At even larger values of ε , the maximum disappears,



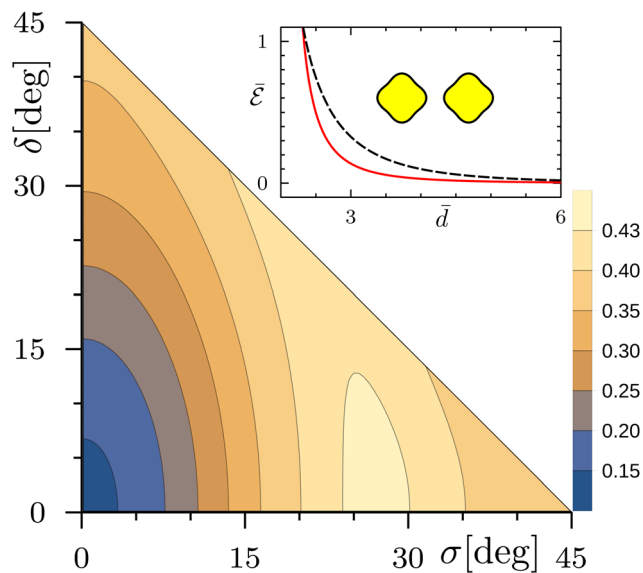


Fig. 11 Same as Fig. 9 but for $\nu = 4$, $\varepsilon = 0.1$ and $M = 40$.

leaving an asymptotic attractive behavior separated from a short distance repulsion by a minimum, as for $\nu \leq 3$.

5.5 Convergence of the numerical algorithm

As we discussed in Sec. 3, we throughout check the convergence of our numerical algorithm by increasing the maximum order M of the multipoles (along with the maximum order P of the Fourier harmonics). Usually, as we increase M , the interaction energy first tends to stabilize toward a plateau, allowing to estimate the numerical error. By further increasing M (above a few hundreds for two circular inclusions), the numerical error tends to increase again for numerical stability reasons, as is usually the case.

However, for a given number of lobes ν , we find that when increasing the amplitude ε , the algorithm does not converge

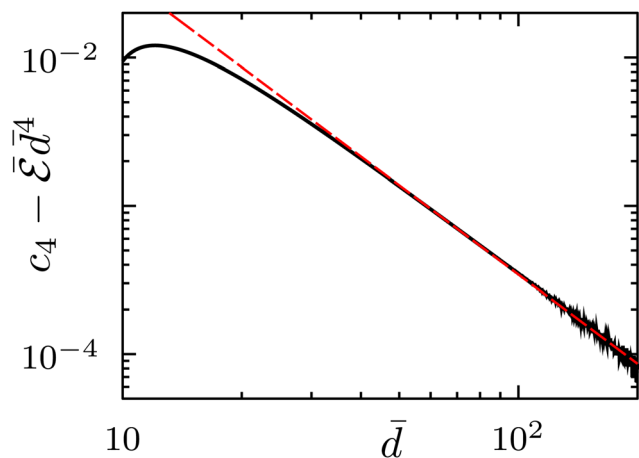


Fig. 12 Asymptotic interaction energy for $\nu = 4$ and $\varepsilon = 0.1$ as a function of the normalized distance \bar{d} . Black solid line: $c_4 - \bar{\varepsilon} \bar{d}^4$ with $c_4 = 6.819842$. Red dashed line: $-c_6 \bar{d}^{-2}$, with $c_6 = -3.44$. The \bar{d}^{-2} asymptotic behavior of $c_4 - \bar{\varepsilon} \bar{d}^4$ shows that $\bar{\varepsilon} = c_4/\bar{d}^4 + c_6/\bar{d}^6 + \dots$ for large \bar{d} .

anymore: as we increase M , the absolute value of the interaction energy $\bar{\varepsilon}$ continuously increases. The maximum amplitude ε_{\max} for which the algorithm converges decreases as ν increases and also slightly decreases as the distance \bar{d} decreases. For instance, close to contact, $\varepsilon_{\max} \approx 0.25$ for $\nu = 2$, while $\varepsilon_{\max} \approx 0.1$ for $\nu = 6$. Indeed, when the inclusions shape presents pronounced lobes, more multipolar expansions inside each inclusions might be necessary to match the boundary conditions on the corrugated contour.

6. Conclusions

In this article, using the disk with detachment angle model of curvature-inducing proteins and the multipolar expansion method originally introduced by Goulian *et al.*,⁴ valid in the limit of small detachment angles, we have studied the interaction between multiple proteins of arbitrary contours and fixed detachment angle in a tensionless membrane. For two identical proteins with circular contour, we have shown numerically, by taking a very large number of multipoles, that the analytical asymptotic interaction of Goulian *et al.*^{4,6} reproduces quite well the exact result up to center-to-center distances of the order of 2.5 times the contour radius, and differs by up to a factor of order 3 at contact.

For $N = 3-6$ proteins with circular contours arranged at the vertices of a regular polygon, we have obtained analytical asymptotic interaction energies. For all values of N but $N = 5$, we have found that the interaction decays as the inverse fourth power of the distance d between nearest neighbor inclusions, as originally found by Goulian *et al.*⁴ for two inclusions. For $N = 5$ proteins, instead, we found that the asymptotic interaction decays as d^{-6} . This result is at variance with the null result of ref. 15, but it is compatible with the findings of Yolcu *et al.*⁸ that the approximation of ref. 15 only takes into account two and three bodies interactions up to the order d^{-4} . We checked numerically these results, using the multipolar technique truncated at an arbitrary high number of contributions up to convergence.

We also computed numerically the different multi-body contributions to the total interaction energy, verifying that the nonpairwise multi-body interactions are indeed generally comparable to the pairwise ones. Apart possibly very close to contact, the multi-body contributions are all attractive, thus reducing the contribution coming from the sum of the two-body terms.

Finally, in the case of two identical proteins, we have numerically studied the effect of a departure of the contour from the circular shape. For the sake of simplicity, we have considered contour shapes that contain a single Fourier harmonic $\nu = 1, 2, \dots$ of relative amplitude ε in their polar coordinate equation, thus consisting of ν identical lobes. For a small number of lobes ($\nu = 1-3$), we found that, whatever the amplitude of the modulation, the interaction becomes asymptotically attractive, decaying as d^{-2} . This is in agreement with previous models of conical transmembrane proteins with



effective non-circular sections,¹⁷ or effective nonuniform detachment angles.^{18,19} Note that for distances comparable to the size of the contours, the interaction remains repulsive. Therefore, contrary to the case of two circular inclusions, for such inclusions the asymptotic interaction does not hold at intermediate distances.

For a larger number of lobes $\nu \geq 4$ and a small modulation amplitude ε , we recovered, on the other hand, the asymptotic repulsive d^{-4} character of the interaction. Above a threshold value of ε (≈ 0.16 for $\nu = 4$), the large distance behavior becomes attractive, with, as for $\nu < 4$, a repulsion for short distances.

For all but the $\nu = 1$ case, we found that the interaction, at fixed distance, is minimized when the lobes of the two inclusions are facing each other. In the $\nu = 1$ case, on the other hand, the minimum configuration remains symmetric with respect to the mid-plane, but the orientation angle depends on the distance. Up to a given distance close to contact, the facing sides of the inclusions are the flattest parts. Then, on increasing the distance, a second-order orientation transition occurs, with the orientation angles of the two lobes with respect to the line joining the two inclusions centers continuously decreasing from π to $\pi/2$ (see Fig. 8). These results are not incompatible with the cases $\nu \neq 1$, since for $\nu = 1$ the protein contour has a maximum curvature not on the tip of the lobe, but on two symmetric points close to the flat side. Therefore, it seems that the configurations that are favored correspond to having the contours maximum curvatures close to each other. This could also explain why, for $\nu = 1$, an antisymmetric metastable configuration, having an interaction energy only slightly larger than the absolute minimum, is present.

Finally, note that the next to leading order of the asymptotic interaction for two perfectly circular inclusions scales as d^{-8} , the d^{-6} contribution being exactly zero. Numerically, we found that this anomaly is due to the perfect rotational symmetry of the inclusions and is lost when the rotational symmetry is broken.

Conflicts of interest

There are no conflicts to declare.

A Appendix

The variation $\delta\mathcal{F}$ of the free energy (1) with respect to arbitrary infinitesimal variations δh of the height of the membrane that respect the boundary conditions on the inclusions is

$$\delta\mathcal{F} = \int (\nabla^4 h) \delta h \, dx dy - \sum_k \left(F_k^z \delta z_k + \mathbf{\Gamma}_k^{\parallel} \cdot \delta \boldsymbol{\omega}_k \right), \quad (24)$$

with

$$F_k^z = -\kappa \oint_{C_k} \frac{\partial}{\partial n_k} (\nabla^2 h) \, ds_k \quad (25)$$

and

$$\mathbf{\Gamma}_k^{\parallel} = \left\{ \kappa \oint_{C_k} \left[\frac{\partial}{\partial n_k} (\nabla^2 h) \mathbf{r}_k - (\nabla^2 h) \frac{\partial \mathbf{r}_k}{\partial n_k} \right] ds_k \right\} \times \hat{\mathbf{z}}. \quad (26)$$

Here $\mathbf{r}_x = x_k \hat{\mathbf{x}}_k + y_k \hat{\mathbf{y}}_k$ is the vector that locates the points of the reference plane with respect to the local coordinate frame associated to inclusion k and $\delta \boldsymbol{\omega}_k$ is the infinitesimal rotation, parallel to the reference plane, of inclusion k .

By the principle of virtual works, F_k^z (resp. $\mathbf{\Gamma}_k^{\parallel}$) is the force (resp. torque) normal (resp. parallel) to the reference plane acting on inclusion k . At equilibrium ($\delta\mathcal{F} = 0$), the forces F_k^z and the torques $\mathbf{\Gamma}_k^{\parallel}$ must vanish.

Let us first consider the force (25). We decompose the total height field h in two terms: the contribution h_k coming from the multipoles centered on the same inclusion k and the contribution \hat{h}_k that is the sum of the multipoles centered on all the other inclusions. Then $F_k^z = \tilde{F}_k^z + \hat{F}_k^z$, with

$$\tilde{F}_k^z = -\kappa \oint_{C_k} \frac{\partial}{\partial n_k} (\nabla^2 h_k) \, ds_k, \quad (27)$$

$$\hat{F}_k^z = -\kappa \oint_{C_k} \frac{\partial}{\partial n_k} (\nabla^2 \hat{h}_k) \, ds_k. \quad (28)$$

Now, given a membrane height field h satisfying the equilibrium condition (2) and an arbitrary contour C on the reference plane, having outward normal $\hat{\mathbf{n}}$ and enclosing a surface S within which h is regular, using the Green theorem, we have

$$\oint_C \frac{\partial}{\partial n} (\nabla^2 h) \, ds = \oint_C \hat{\mathbf{n}} \cdot \nabla (\nabla^2 h) \, ds = \int_S \nabla \cdot \nabla (\nabla^2 h) \, dx dy = \int_S \nabla^4 h \, dx dy = 0, \quad (29)$$

reflecting the fact that the stress tensor is divergenceless.²⁰ If the contour C encloses singularities of the height field h , the line integral on the left-hand side of eqn (29) will be in general different from zero. However, eqn (29) implies that, if such a contour is continuously deformed without crossing any singularity, the value of the line integral will not change. Therefore, if we take as the contour in eqn (27) a circle of any radius r and center on the center of the inclusion, we have

$$\tilde{F}_k^z = -\kappa \int_0^{2\pi} \frac{\partial}{\partial r} (\nabla^2 h_k) r \, d\phi, \quad (30)$$

where (r, ϕ) are polar coordinates centered on the inclusion. Now, according to the multipolar expansion (10),

$$\frac{\partial}{\partial r} (\nabla^2 h_k) = \sum_{m=2}^{\infty} \left[\frac{4m(m-1)L^{m-1}}{r^{m+1}} \left(B_{k,m}^c \cos(m\phi) + B_{k,m}^s \sin(m\phi) \right) \right] \quad (31)$$

and, therefore, the integral in the right-hand side of eqn (30) identically vanishes. Finally, since \hat{h}_k is regular inside inclusion k , according to eqn (29) $\hat{F}_k^z = 0$.

To conclude, whatever the constant coefficients $A_{k,m}^c$, $A_{k,m}^s$, $B_{k,m}^c$ and $B_{k,m}^s$, the membrane profile (10) does not exert on the inclusions any force normal to the reference plane.



Let us now consider the torque (26). The vector in curly braces in eqn (26) is proportional to

$$\mathbf{L} = \sum_{i=1}^2 L_i \hat{\mathbf{x}}^{(i)}, \quad (32)$$

$$L_i = \oint_C \left[\frac{\partial}{\partial n} (\nabla^2 h) x^{(i)} - (\nabla^2 h) \frac{\partial x^{(i)}}{\partial n} \right] ds, \quad (33)$$

where $x^{(1)} = x$, $x^{(2)} = y$, $\hat{\mathbf{x}}^{(1)} = \hat{\mathbf{x}}$, $\hat{\mathbf{x}}^{(2)} = \hat{\mathbf{y}}$, and the contour C coincides with the contour C_k of inclusion k . Let us now show that, similarly to eqn (29), the line integrals (33) are zero if the height field h satisfies the equilibrium condition (2) and is regular inside C . To this aim, let us first note that

$$\frac{\partial x^{(i)}}{\partial n} = \hat{\mathbf{n}} \cdot \nabla x^{(i)} = \hat{\mathbf{n}} \cdot \hat{\mathbf{x}}^{(i)}. \quad (34)$$

Then, using the identity,

$$\frac{\partial}{\partial n} (\nabla^2 h) x^{(i)} - (\nabla^2 h) \frac{\partial x^{(i)}}{\partial n} = \frac{\partial}{\partial n} (x^{(i)} \nabla^2 h) - 2 \hat{\mathbf{n}} \cdot \hat{\mathbf{x}}^{(i)} \nabla^2 h \quad (35)$$

and the Green theorem, to convert the line integral along C of the first term on the right-hand side of eqn (35) to a surface integral over the enclosing surface S , we get

$$L_i = \int_S \nabla \cdot \nabla (x^{(i)} \nabla^2 h) dx dy - 2 \oint_C \hat{\mathbf{n}} \cdot \hat{\mathbf{x}}^{(i)} \nabla^2 h ds. \quad (36)$$

We note that

$$\nabla \cdot \nabla (x^{(i)} \nabla^2 h) = \nabla^2 x^{(i)} \nabla^2 h + 2 \nabla x^{(i)} \cdot \nabla (\nabla^2 h) + x^{(i)} \nabla^4 h. \quad (37)$$

Since $\nabla^2 x^{(i)} = 0$, $\nabla x^{(i)} = \hat{\mathbf{x}}^{(i)}$, $\nabla^4 h = 0$, and, being $\nabla \cdot \hat{\mathbf{x}}^{(i)} = 0$, $\hat{\mathbf{x}}^{(i)} \cdot \nabla (\nabla^2 h) = \nabla \cdot (x^{(i)} \nabla^2 h)$, using the Green theorem we then obtain

$$\int_S \nabla \cdot \nabla (x^{(i)} \nabla^2 h) dx dy = 2 \oint_C \hat{\mathbf{n}} \cdot \hat{\mathbf{x}}^{(i)} \nabla^2 h ds. \quad (38)$$

Inserting this latter equation in the first term on the right-hand side of eqn (36), finally proves that the torque (26) is zero for any height field h satisfying the equilibrium condition (2) and regular inside the contour C_k . Using now the same decomposition as in eqn (27) and (28) and the same steps, one

can readily see that, whatever the constant coefficients $A_{k,m}^x$, $A_{k,m}^y$, $B_{k,m}^x$ and $B_{k,m}^y$, the membrane profile (10) does not either exert on the inclusions any torque parallel to the reference plane.

Notes and references

- 1 H. Lodish *et al.*, *Molecular Cell Biology*, W. H. Freeman & Co, New York, 7th edn, 2012.
- 2 S. Aimon, A. Callan-Jones, A. Berthaud, M. Pinot, G. E. S. Toombes and P. Bassereau, *Dev. Cell*, 2014, **28**, 212–218.
- 3 W. Helfrich, *Z. Naturforsch. C*, 1973, **28**, 693.
- 4 M. Goulian, R. Bruinsma and P. Pincus, *EPL*, 1993, **22**, 145.
- 5 M. Goulian, R. Bruinsma and P. Pincus, *EPL*, 1993, **22**, 155.
- 6 J.-B. Fournier and P. G. Dommersnes, *EPL*, 1997, **39**, 681.
- 7 C. Yolcu, I. Z. Rothstein and M. Deserno, *Phys. Rev. E*, 2012, **85**, 011140.
- 8 C. Yolcu, R. C. Haussman and M. Deserno, *Adv. Colloid Interface Sci.*, 2014, **208**, 89–109.
- 9 J.-B. Fournier and P. Galatola, *Eur. Phys. J. E: Soft Matter Biol. Phys.*, 2015, **38**, 86.
- 10 B. Reynwar, G. Illya, V. Harmandaris, M. Muller, K. Kremer and M. Deserno, *Nature*, 2007, **447**, 461.
- 11 B. J. Reynwar and M. Deserno, *Soft Matter*, 2011, **7**, 8567–8575.
- 12 Y. Schweitzer and M. Kozlov, *PLoS Comput. Biol.*, 2015, **11**, e1004054.
- 13 A. H. Bahrami and T. R. Weikl, *Nano Lett.*, 2018, **18**, 1259–1263.
- 14 P. Bassereau, Private communication.
- 15 K. S. Kim, J. Neu and G. Oster, *Biophys. J.*, 1998, **75**, 2274.
- 16 T. R. Weikl, M. M. Kozlov and W. Helfrich, *Phys. Rev. E*, 1998, **57**, 6988–6995.
- 17 Jeong-Man Park and T. C. Lubensky, *J. Phys. I France*, 1996, **6**, 1217–1235.
- 18 P. G. Dommersnes and J.-B. Fournier, *Eur. Phys. J. B*, 1999, **12**, 9–12.
- 19 J. A. Kwiecinski, A. Goriely and S. J. Chapman, *SIAM J. Appl. Math.*, 2020, **80**, 2448–2471.
- 20 J.-B. Fournier, *Soft Matter*, 2007, **3**, 883–888.

